ACS NANO

www.acsnano.org

ARTICLE

Stimulated Nucleation of Skyrmions in a Centrosymmetric Magnet

Binbin Wang, Po-kuan Wu, Núria Bagués Salguero, Qiang Zheng, Jiaqiang Yan, Mohit Randeria, and David W. McComb*

Cite This: *ACS Nano* 2021, 15, 13495−13503

Read Online

ACCESS | Metrics & More | Article Recommendations | Supporting Information

ABSTRACT: **Understanding the dynamics of skyrmion nucleation and manipulation is important for applications in spintronic devices. In this contribution, the spin textures at magnetic domain-boundaries stimulated by application of in-plane magnetic fields in a centrosymmetric kagome ferromagnet, Fe_3Sn_2, with thickness gradient are investigated using Lorentz transmission electron microscopy. Switching of the in-plane magnetic field is shown to induce a reversible transformation from magnetic stripes to skyrmions, or *vice versa*, at the interface between differently oriented domains. Micromagnetic simulations combined with experiments reveal that the rotatable anisotropy and thickness dependence of the response to the external in-plane field are the critical factors for the skyrmion formation. In addition, it is shown that the helicity of skyrmions can also be controlled using this dynamic process. The results suggest that magnetic materials with rotatable anisotropy are potential skyrmionic systems and provides a different approach for nucleation and manipulation of skyrmions in spintronic devices.**

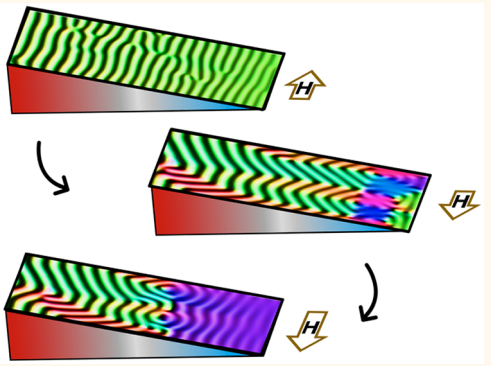

KEYWORDS: *centrosymmetric magnets, skyrmions, spintronic devices, thickness gradient, in-plane fields, Lorentz TEM, Fe_3Sn_2*

Magnetic skyrmions are topologically protected particle-like spin textures that exist in several magnetic materials. Much skyrmion research has been focused on magnetic materials with broken inversion symmetry, where the Dzyaloshinskii−Moriya interaction (DMI) can be induced/adjusted to stabilize skyrmions with the assistance of external fields.[1,2] Skyrmions in centrosymmetric materials can be stabilized by other mechanisms such as long-range dipolar interactions, competing exchange interactions, and four-spin exchange interactions.[1,3,4] Furthermore, skyrmions in centrosymmetric magnets can host a rich array of spin textures, since they have a helicity/vorticity degree of freedom due to the absence of DMI.[4−6] Skyrmions in such materials often exhibit better thermal stability due to higher magnetic ordering temperatures and stronger exchange interactions compared with DMI controlled systems.[5,7] For example, skyrmion bubbles and target skyrmions have been identified in a frustrated kagome magnet, Fe_3Sn_2, over a record stable temperature range, 130−630 K.[8−10] However, compared to materials with DMI, the higher magnetic fields necessary for nucleation of skyrmions in centrosymmetric magnets limit their applications.[6,7,9,11,12] To overcome this, methods such as geometric confinement,[13,14] temperature switching,[10] or stimulations such as applied current[15,16] and laser excitation[17] have been explored.

In this contribution, the dynamic switching of an applied in-plane magnetic field is used to nucleate and manipulate magnetic textures in Fe_3Sn_2—a material that has attracted much interest due to its unusual physics and exotic correlated phenomena.[18−20] Lorentz transmission electron microscopy (LTEM) is utilized for *in situ* observation of the magnetic textures. It is shown that dynamic switching of a weak in-plane magnetic field can be used to induce reorientation of magnetic textures, resulting in an unexpected magnetic texture transformation from magnetic stripes to skyrmions, and *vice versa*, when geometrical asymmetry involved. In the current work, both bubbles and target skyrmions are observed in both experiment and simulation. The connection between in-plane field induced transformation and magnetic stripe domains suggests the class of materials that can host skyrmions may be extended to other centrosymmetric magnets with rotatable anisotropy. Furthermore, it is shown that the helicity of skyrmions can also be

Received: May 12, 2021
Accepted: August 5, 2021
Published: August 10, 2021

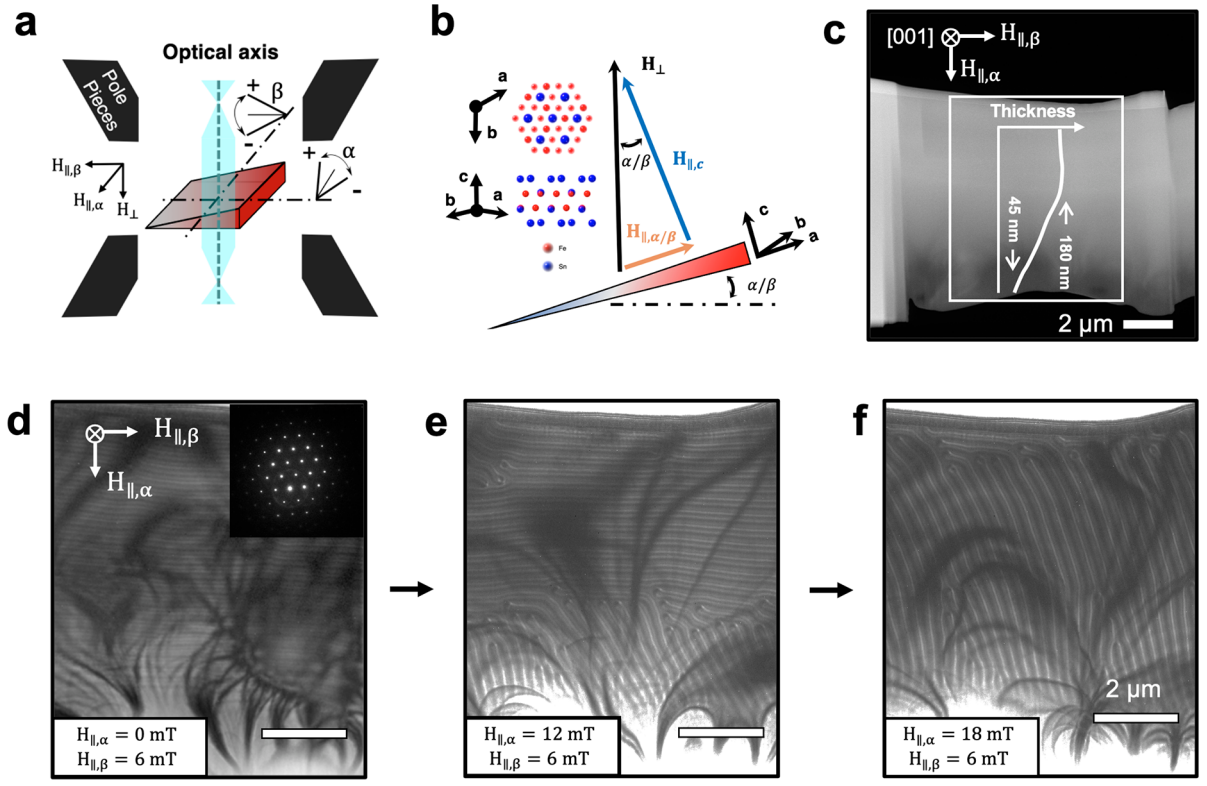

Figure 1. Thickness and in-plane field dependence of magnetic stripe reorientation. (a) Schematic diagram of the experimental setup in the TEM. (b) Diagram for the formation of in-plane fields $H_{\|,\alpha}$ or/and $H_{\|,\beta}$ due to sample tilt along the α or/and β direction. The crystal structures of Fe_3Sn_2 are inserted to illustrate the relative direction between the magnetic fields and crystal structure in the sample. (c) ADF-STEM image of the focused ion beam (FIB) prepared sample exhibiting a thickness profile along the $H_{\|,\alpha}$ direction. (d–f) Overfocused LTEM images of the rectangular selected region in (b) recorded under a normal field of 70 mT show changes in the magnetic configurations as the in-plane field is altered by sample tilting: (c) $\alpha = 0°$, $\beta = 5°$; (d) $\alpha = 10°$, $\beta = 5°$; (e) $\alpha = 15°$, $\beta = 5°$. The inset in (d) is an example of the diffraction pattern acquired along the (c) direction of Fe_3Sn_2.

influenced using dynamic switching of in-plane fields, providing an approach to control skyrmionic textures.

RESULTS AND DISCUSSION

In LTEM, the objective lens (O.L.) is normally switched off so that the specimen, which is positioned between the upper and lower electromagnetic polepieces, is in a field-free environment. In this study, the specimen is loaded into the microscope with the O.L. switched off and then weakly excited to apply a small magnetic field (~70 mT) normal to the specimen (Figure 1a). If the specimen is tilted with respect to this normal along one of the two orthogonal tilt axes (α and β), an in-plane magnetic field results with a component aligned with the direction of the tilt, $H_{\|,\alpha}$ and $H_{\|,\beta}$ (see Figure 1b). In the current study, an electron transparent specimen of Fe_3Sn_2 was prepared along the [001] direction from a liquid transport grown single crystal by focused ion beam milling; see Methods. In each experiment, the sample was aligned in the [001] direction by the diffraction pattern and Ronchigram. From this starting position, the in-plane field strength and direction in the *ab* plane was controlled by tilting the sample on two orthogonal tilt axes (α and β) and rotating the sample around the *c* axis using a double tilt rotation analytical TEM specimen holder. In-plane field strengths are calculated based on the geometric relationship between sample tilt angles and the normal field whose strength is tunable by the O.L. current. An annular dark field (ADF) scanning transmission electron microscope (STEM) image is shown Figure 1c, with an indicated thickness gradient as determined by electron energy loss spectroscopy (EELS). To define the starting point for the experiment, a 5° tilt on the β-tilt axis is used to apply an in-plane field to align the magnetic stripe phase along this axis (Figure 1d). While maintaining $\beta = 5°$, the tilt on the orthogonal α-axis is increased stepwise from 0° to 15°. The observed LTEM images (Figure 1d–f) show a reorientation of magnetic stripes, initially in the thinnest region and continuing to thicker regions, as the in-plane magnetic field $H_{\|,\alpha}$ increases. The spin direction in these stripes can be determined from the LTEM contrast.[14,21] This kind of magnetic stripe reorientation has been reported previously in magnets with "rotatable anisotropy" where the threshold field for reorientation is related to the perpendicular magnetic anisotropy (K_{PMA}) energy density.[22−25]

Micromagnetic modeling reveals that the competition of exchange constant (A_{ex}), K_{PMA}, M_S, and the sample thickness determines the width of stripes and threshold fields for their reorientation, *i.e.*, rotatable anisotropy. Details of the simulations can be found in the Methods section. As shown in Figure 2, the periodicity of the stripe phase is strongly dependent on thickness. It is observed that the pitch length λ decreases with decreasing t or decreasing A_{ex}. There exists a critical thickness $t_c \propto \sqrt{A_{ex}}$ such that the stripe phase is unstable for $t < t_c$, and there is a saturated ferromagnetic phase with in-plane magnetization (Figure S1, Supporting Information). As t decreases, there are two consequences: (i) λ decreases, and (ii) the in-plane component of spins increases. In addition, the stripe pitch length has a corresponding critical value $\lambda_c \sim t_c$ and the stripes become less stable as t approaches t_c. The instability and larger in-plane

https://doi.org/10.1021/acsnano.1c04053
ACS Nano 2021, 15, 13495−13503

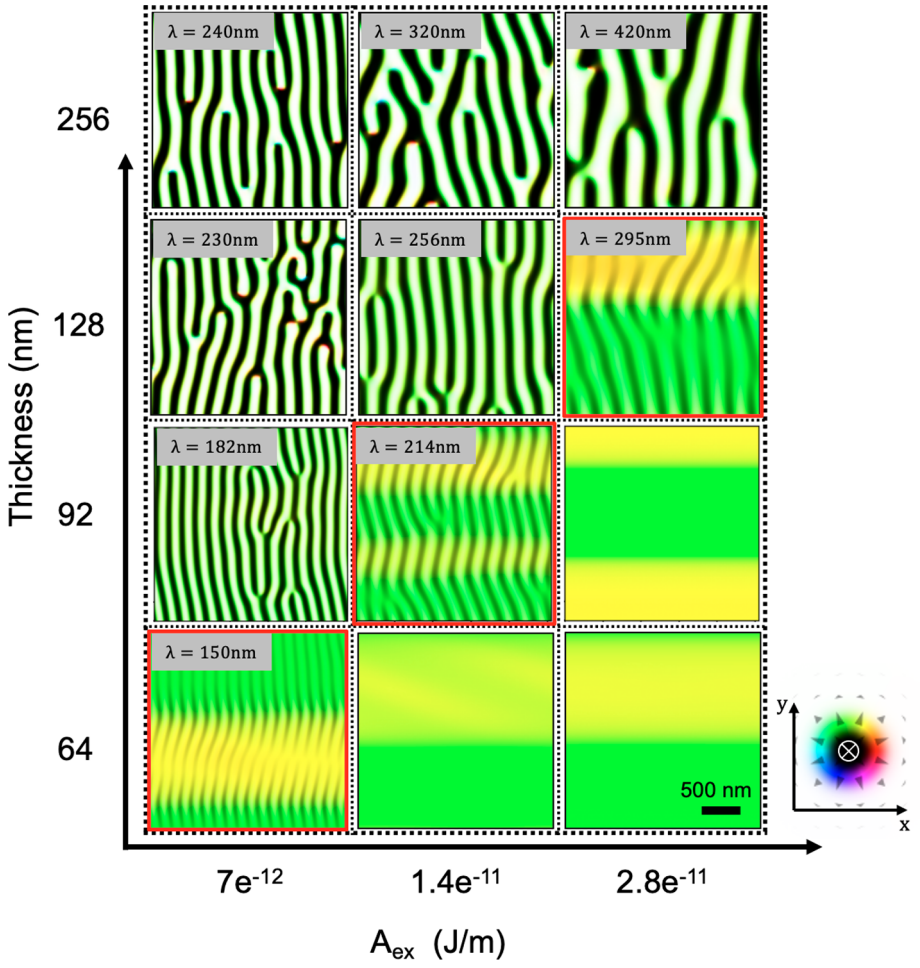

Figure 2. Micromagnetic simulations of the thickness dependence of the magnetic stripe pitch length λ with different exchange constant A_{ex}. The configurations with a red outline show the configurations at t_c and corresponding pitch length λ_c for different values of A_{ex}. The value of pitch length is obtained by the Fourier transform of the configuration. Color saturation indicates that the in-plane magnetic component increases as thickness decreases.

spin component cause a stronger response to the in-plane field for the system with a smaller thickness. The weaker threshold field in the thinner region is due to the increase of the in-plane component of spins resulting in decreased stripe widths and saturation field (M_S); see Figure S2. The trend of variation of the stripe width is consistent with observations in geometrically confined Fe_3Sn_2.[14]

To nucleate skyrmions in magnetic materials, the external magnetic field is usually applied along the easy axis of the material.[1,2,26] In the absence of geometric confinement, the critical field for nucleation of isolated skyrmions in Fe_3Sn_2 is ~800 mT.[9] Simulations indicate that there is a critical sample thickness, ~150 nm,[14] below which increasing magnetic field would make the stripe domains transform directly to a magnetic saturation state without formation of the skyrmion phase. This was experimentally confirmed in our sample (see Figure S3). In this work, we demonstrate stimulated nucleation of skyrmions in a sample below the critical sample thickness when the in-plane field direction is switched (Movie S1). In this experiment, the sample has a thickness gradient aligned along the β-tilt axis with an average thickness of ~100 nm. The in-plane field switching was achieved in the LTEM by continuously tilting the sample in both positive and negative directions along the α-tilt axis to create a dynamically varying in-plane magnetic field that reverses direction at 0° tilt angle within a normal field fixed at 20 mT. In this process, skyrmions are observed to nucleate/annihilate at the boundary created by the oscillating in-plane field between two different oriented magnetic stripe domains. The LTEM images in Figure S4 show the dependence of the magnetic texture transformation on the magnetic field strength during the in-plane field oscillation. The highest density of transformation events is observed when the normal field is ~20 mT, corresponding to an in-plane field ~5 mT. We note that conventional domain walls form in the field switching process, which may be associated with FIB preparation artifacts such as surface amorphization, material redeposition, and sample bending (as shown in Figure 1d and Figure S3).

To investigate the origin of the skyrmion nucleation, the influence of higher applied fields was investigated. Initially, the magnetic stripe phase was aligned along the β-tilt axis by application of a saturation magnetic field with β-tilt axis of 2°; see Figure 3a. The normal magnetic field was then decreased to 30 mT while maintaining β = 2°. An oscillating in-plane field $H_{\parallel,\alpha}$, ±7.8 mT, was created by continuously oscillating the specimen ±15° along the α-tilt axis. After the in-plane field oscillation, the initial magnetic stripe phase is transformed to mixed magnetic textures with a rich array of magnetic textures (Figure 3b) with a skyrmion coexisting with two types of magnetic stripes (type I and type II) decorated with π Bloch lines (π-BLs).[21,27] The type I stripes are defined as the narrow

https://doi.org/10.1021/acsnano.1c04053
ACS Nano 2021, 15, 13495−13503

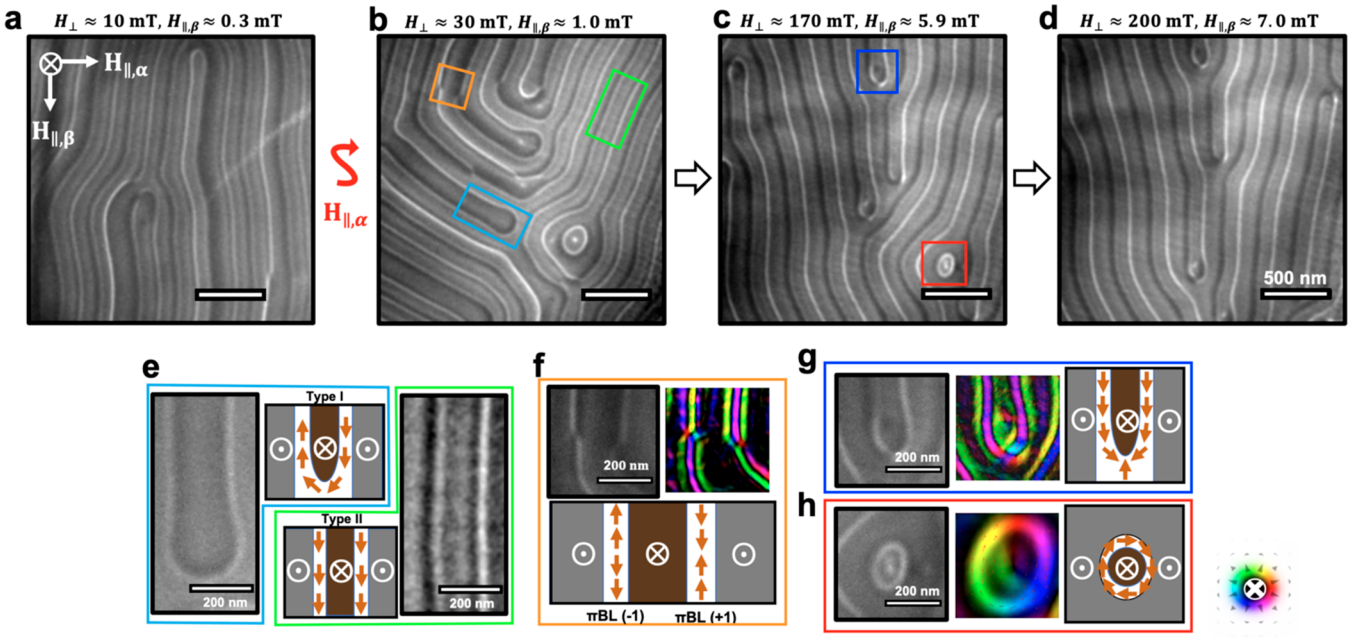

Figure 3. Evolution of mixed magnetic textures after in-plane field oscillation. (a) Defocused LTEM image of Fe_3Sn_2 in a residual field (~10 mT) with stripes initially aligned to β-tilt axis. (b) Defocused LTEM image of the resulting mixed magnetic textures after a period of in-plane field oscillation of $H_{\parallel,\alpha}$ ($\lesssim$7.8 mT) under a normal field of 30 mT. The evolution of the mixed magnetic textures in (b) under increased normal fields: (c) 170 mT and (d) 200 mT. (e–h) Magnified images of the magnetic structure indicated by boxes in (b,c) and schematics illustrating their corresponding magnetization textures. Type I and type II stripes highlighted in (e); π-BLs with different magnetic charges in (f); paired strips jointed with a π-BL in (g); and a skyrmion in (h), where the vortex-like contrast visible in the center of the bubble originates from the 3D nature of magnets.[8,10] The arrows in magnetization textures indicate the direction of in-plane magnetizations of the magnetic textures (the color in magnetization textures mapping indicated by the color wheel), while the darkness indicates out-of-plane magnetizations as the region indicated with gray and brown colors in the schematic drawing.

stripe domains bounded by antiparallel Bloch walls, while the one for type II stripes is bounded by two parallel Bloch walls (Figure 3e), and Bloch lines that with the spin rotation ±180° across each line are named the π-BLs (Figure 3f).[21] While maintaining $\beta = 2°$, the evolution of the mixed magnetic textures was investigated as the magnitude of the normal magnetic field was increased to 170 and 200 mT, which corresponds to in-plane fields along the β-tilt axis of 5.9 and 7.0 mT, respectively (Figure 3c,d). Under these conditions, the type II stripes became dominant. They tend to align parallel to the in-plane field and are terminated by π-BLs (Figure 3g). Increasing the in-plane fields moves the π-BLs with opposite topological charge to opposite directions in domain walls. This suggests that the skyrmion nucleated is not created by pair-annihilation of two π-BLs with opposite topological charges under the increasing normal magnetic fields as reported in other magnets.[11,14,21,28]

Figure 3 also demonstrates the robustness of the skyrmions to applied external fields, as skyrmions nucleated in this approach not only exist under zero-field, but remain at the higher magnetic field. Furthermore, the radii of the skyrmions decreases as the external magnetic field strength increases. As shown in Figure 3c, despite an elongation in the in-plane field direction, the skyrmion still shows topological integrity at 170 mT with average radius (72 ± 13 nm) that is about half the size of skyrmions (~130 nm) reported in previous studies at 140 mT.[14] The skyrmion size in centrosymmetric magnets is determined by the competition of A_{ex}, K_{PMA}, and M_S, which can be thickness-dependent. Our observations show that it is possible to control the size of target skyrmions using these parameters.

The dynamic process of transformation from stripe domains to skyrmions and *vice versa* was probed in the LTEM. The types of magnetic texture observed are highly sensitive to small changes of the in-plane field (examples of such transformations can be found in Figure S5). However, since it is a dynamic process (Movies S5 and S6), obtaining high resolution and focal series images with clear magnetic contrast at each value of the in-plane field is challenging and limits the ability to accurately identify each magnetic texture observed. To overcome this and confirm the role of in-plane fields in the dynamic switching process, micromagnetic simulations were performed (details in Methods). A sample, 5 × 2.5 μm, with a thickness gradient from 128 to 90 nm along the x-axis was simulated. The initial stripe phase in Figure 4a was aligned along the y-direction by annealing in an in-plane field H_y that was lowered from 100 mT down to 2 mT. As shown in Figure 2, with decreasing sample thickness, (i) a decreasing stripe pitch, and (ii) an increasing in-plane magnetization were observed. The latter is directly responsible for making the thinner region more sensitive to in-plane fields. Next, the field, H_y, was reversed, switching from 2 mT to −10 mT. The thinner part of the sample begins to show a strong response when H_y is around −7.3 mT (Figure 4b), where one can see the in-plane component distortion due to in-plane field inversion. Since stripes parallel to the in-plane field direction are energetically favorable, we observed stripe direction inversion starting from the thinner end around −7.6 mT forming a target-like skyrmion array with paired skyrmion in opposite helicity (Figure 4c). Increasing in plane field to −8.0 mT will annihilate skyrmions with anticlockwise helicity and a domain wall forms between these "reversed" stripes (near the thin end of the sample) and the original stripes (in the thick part). The field-induced inversion of the in-plane component of the magnetization and its interplay with dipolar interactions leads to the

https://doi.org/10.1021/acsnano.1c04053
ACS Nano 2021, 15, 13495−13503

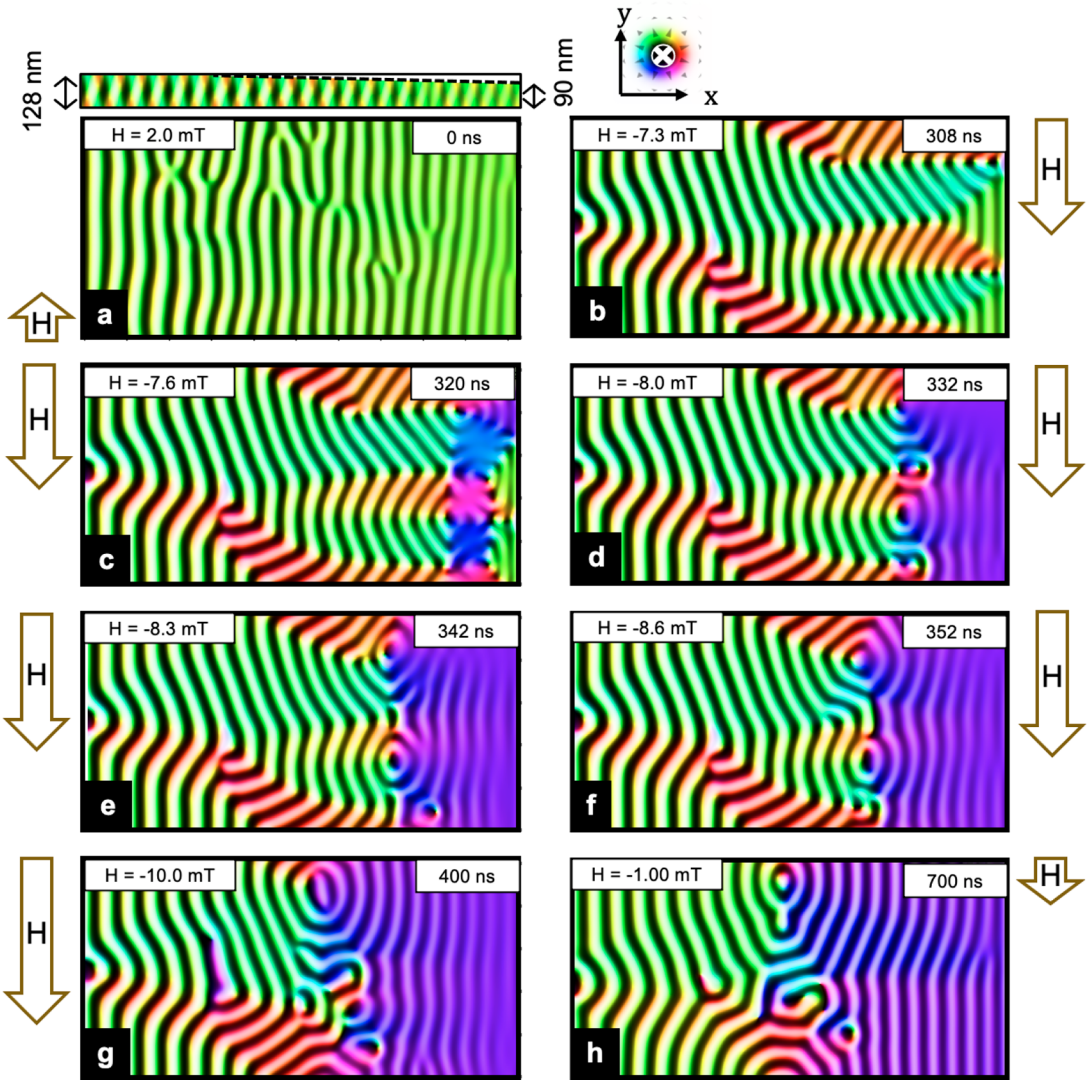

Figure 4. Snapshots of dynamic transformations between magnetic bubbles and stripes from micromagnetic simulation Movie S2, while the external field gradually changes from 2 mT to −10 mT in the *y* direction in 400 ns. The color in images indicates spin directions as shown in the color wheel, while the darkness/white indicates out-of-plane magnetizations. (a) Initial stripe at 0 ns parallel states after annealing from a strong field to 2 mT and equilibrated. The initial configuration is prepared with field annealing from strong in-plane field along the +*y* direction. The inset above, which is the cut view, shows the thickness gradient (from 128 to 90 nm) for simulation setup. (b−h) Snapshots at 308, 320, 332, 342, 352, 400, and 700 ns (corresponding fields are shown in the figures).

creation of skyrmions near the boundary of domains as shown in Figure 4d. It was noted that some of the nucleated skyrmions are unstable and annihilated as the inverted stripe domain expands. However, as observed in Figure 4e, skyrmions with clockwise helicity survived at higher field but are pushed to the thicker region. As the field increases, the in-plane inversed domain grows into the thicker region, and the skyrmion region also moves in this direction (Figure 4f). In this process, long-lived skyrmions can survive when the domain wall stops moving after the final value $H_y = -10$ mT of the external field is reached (Figure 4g). After that, the external field is tuned back to −1 mT, but the domain boundary and skyrmions remain stable, consistent with the experimental results (Figure 4h). Furthermore, skyrmions nucleated in thicker region are more robust to in-plane fields than their counterparts in thinner regions.

It is clear that the thickness gradient plays an important role for both skyrmion nucleation and stability. While a gradient is necessary to nucleate skyrmions, too large a gradient will lead to a short skyrmion lifetime. The simulations in movies (Movies S2, S3) have different thickness gradients (see Figure S7), and the thickness increases from right to left in the images. In the simulation Movie S2, some skyrmions are stable for hundreds of seconds as the in-plane field is reduced, while the skyrmions are unstable in Movie S3. These differences arise from different thickness gradients. In Movie S2, the gradient is about half of that in Movie S3. The smaller gradient provides a larger region for skyrmions to survive near the domain boundary. One can also see a larger intermediate region in the Movie S2, which allows stripes to distort and forms complicated textures such as swirls and target skyrmions. In contrast, the larger gradient provides only a narrow region between domains, and the skyrmion lifetime is decreased.

The skyrmion formation time scale of the varying in-plane field has also been studied in modeling. In Movies S2 and S4, we applied different time scales of varying fields. In Movie S4, it takes 800 ns for the field to change from 2 mT to −10 mT, which

https://doi.org/10.1021/acsnano.1c04053
ACS Nano 2021, 15, 13495−13503

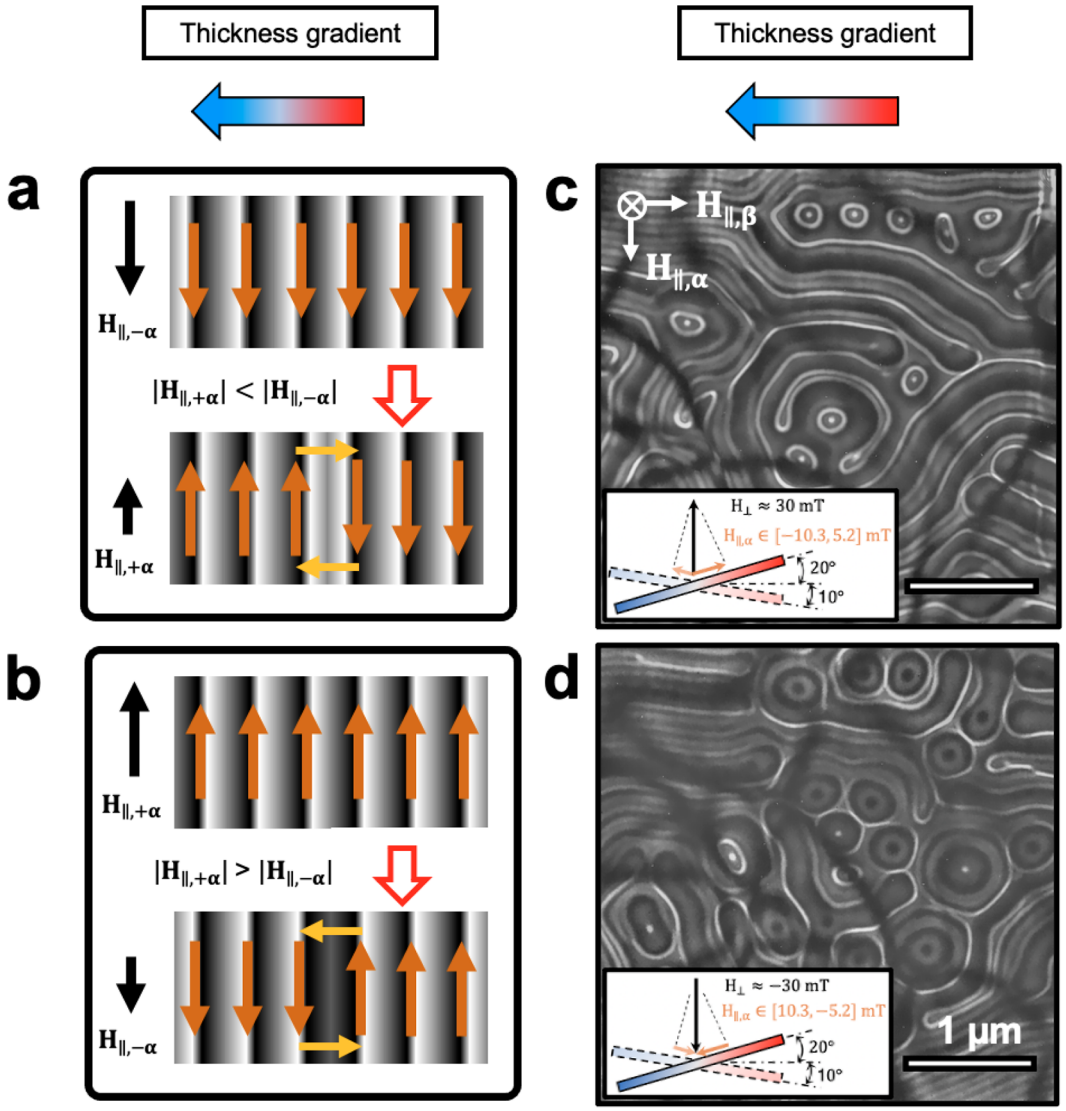

Figure 5. Controlled nucleation of skyrmion using in-plane fields. (a,b) Models for the nucleation of skyrmion with clockwise and anticlockwise helicity at a sample with thickness gradient when domain boundary formed by an asymmetric inversion of the in-plane fields. The direction and magnitude of the in-plane field are indicated by the black arrows, while the brown/yellow arrows indicate correspondence of the in-plane magnetizations with the LTEM contrast (black/white lines). (c,d) Corresponding experimental demonstration of the helicity inversion on a sample with thickness gradient by in-plane field oscillation along $H_{\parallel,\alpha}$ [−10.3, 5.2] mT in (c) and [−5.2, 10.3] mT in (d) by changing the direction of normal field $H_\perp$ of 30 mT.

is twice the time scale in Movie S2. Although our simulations are limited by time and computational power to the same time scale as experiments, qualitative study of the trend gives us insight into the mechanism. We can find that the stripes are more ordered and fewer skyrmions are stabilized. This is consistent with the experimental observation that skyrmions are easy to nucleate under a rapidly switching field.

The result of the micromagnetic simulations provides insight into the connection between the nucleation process and the helicity of the skyrmion formed. In Figure 5a, the stripes are initially aligned to the $(-\alpha)$-direction under $H_{\parallel,-\alpha}$. When a weaker magnetic field $H_{\parallel,+\alpha}$ is applied in the opposite direction, the stripes in the thin region reorient to the $(+\alpha)$-direction. Therefore, a stripe domain boundary forms perpendicular to the thickness gradient direction because the reorientation critical field is thickness dependent as shown in Figure 1 and micromagnetic simulations. In this dynamic process, the domain boundary (type I stripe) transforms to a skyrmion with clockwise (CW) helicity under the dipole−dipole interactions, because spin helices with the opposite direction of magnetization tend to attract each other.[14] Changing the relative strength of the in-plane field and the sequence can reverse the skyrmion helicity to anticlockwise (ACW), as shown in Figure 5b. An experimental demonstration of helicity control is shown in Figure 5c,d. The specimen has a thickness gradient aligned along the β-tilt direction, and the in-plane field will be oscillated in the orthogonal direction, *i.e.*, aligned with the α-tilt axis. The starting point for this experiment is that the sample is tilted +5° along the α-tilt axis. Consequently, an oscillation of ±15° α-tilt corresponds to a tilt ranging from −10° to +20° relative to the normal direction. This means that maximum in-plane field is asymmetric, varying in magnitude by ∼5 mT under a normal field of 30 mT. When the direction of normal field is reversed, *i.e.*, −30 mT, the magnitude of the asymmetric in-plane field is also reversed. The results show that the majority of the skyrmionic bubbles nucleate with opposite helicity when the

https://doi.org/10.1021/acsnano.1c04053
ACS Nano 2021, 15, 13495−13503

relative strength of the in-plane fields along opposite tilt directions are reversed. Some exceptions may arise because of microstructural defects and sample inhomogeneities such as thickness variations or bending, but skyrmion types can be controlled by thickness gradient as discussed in modeling at varied thickness gradient.

CONCLUSIONS

The magnetic texture transformation in a centrosymmetric magnet Fe_3Sn_2 with an engineered thickness gradient has been investigated using LTEM and a strategy for skyrmion nucleation is reported. We have demonstrated that by switching in-plane magnetic field it is possible to nucleate and manipulate skyrmion at values much lower than the reported critical magnetic field for this material. This can lead to potential spintronic devices, *e.g.*, an asymmetric response to the field could be exploited to nucleate a skyrmion which could be injected onto a racetrack device using an electric current. Micromagnetic simulations and associated experiments reveal that the thickness dependence of the response to the external in-plane field is the main factor for the skyrmion formation. The observations reported indicate that magnets with rotatable anisotropy could be a promising class of skyrmionic materials. Meanwhile, the skyrmions nucleated using the method presented here can be much smaller than those reported previously, since pitch length decreases with decreasing thickness. Although such transformations are sensitive to in-plane fields, the skyrmions nucleated in this process are robust to magnetic field in the normal direction, and their size, type, and stability are tunable by geometric engineering.

METHODS

Single Crystal Growth. Single crystals of Fe_3Sn_2 were grown out of Sn flux using a liquid transport growth technique.[29] The starting materials are Fe pieces (Alfa Aesar, 1−3 mm, 99.98%) and Sn shot (Alfa Aesar, 99.9999%). Fe pieces (10 g) and 60 g of Sn were sealed under vacuum in a quartz tube of 19 mm outer diameter and 1.5 mm wall thickness. The growth ampule was then put in a single zone tube furnace with the Fe pieces located at the hot end, *i.e.*, the center of the tube furnace. During the crystal growth, the hot end was kept at 802 °C and the cold end at 782 °C. Two weeks later, the furnace was powered off. Sn flux was then carefully removed by dissolving in HCl acid.

TEM Sample Preparation. The samples for LTEM observations were prepared parallel to the (001) plane from Fe_3Sn_2 single crystals using a FEI Helios NanoLab 600 DualBeam focused ion beam (FIB). The thickness gradient was prepared in the final thinning process in FIB and then measured using electron energy loss spectroscopy (EELS) on an image-corrected Titan G2 60−300 S/TEM at 300 kV. To obtain the absolute thicknesses of TEM samples, the mean free path for inelastic scattering was estimated using the program IMFP.[30]

LTEM Measurements. LTEM imaging was carried out in Fresnel mode by using an image-corrected Titan3 G2 60−300 S/TEM at 300 kV. The *in situ* process was recorded using a Gatan K2 Summit electron counting direct detection camera with a frame rate of 40 fps. In LTEM, the objective lens was switched off, leaving the sample in a nominally field-free environment (a small remnant field, ∼10 mT, could remain). By varying the objective lens strength, a magnetic field parallel to the electron beam could be applied. A TEM sample rod with a Hall sensor was used to calibrate the magnetic field applied to the sample. The magnetic field is mostly applied normal/out-of-plane respect to the sample. By tilting the sample, an in-plane field can be also applied. In that case, the total magnetic field is composed by an in-plane and an out-of-plane field. A double tilt rotation analytical holder from Gatan (model 925) was used to control the magnitude and direction of the in-plane magnetic field component applied to the sample. In LTEM, the electron beam is deflected due to the interactions between incident electrons and in-plane magnetic moments of the sample. On the under/overfocus LTEM images, bright or dark contrast related to the convergent or divergent electron beam, which reflects the in-plane magnetizations components in sample. The defocus values are varied in the range 300−600 μm during the experiment to optimize the magnetic contrast. The determination of in-plane spin direction of the stripe walls is determined using magnetization maps. These are obtained from LTEM focal series images acquired then reconstructed using the software package QPt which is based on transport-of-intensity equation (TIE).[31] In the resulting magnetization maps, the dark region represents out-of-plane magnetization. In addition, nonlocal means filtering, and background flattening was used in some experimental images to reduce noise and enhance contrast.

Micromagnetic Simulation. In our micromagnetic simulations, performed using Mumax3, we studied two questions: (1) formation of skyrmions and (2) 2idth of stripes. For both cases, we used the following parameters: saturation magnetization M_s = 556 kA/m and uniaxial anisotropy $K_u = 45\ kJ/m^3$ for the simulation on the formation of skyrmions. The simulations for skyrmion formation have exchange stiffness $A_{ex} = 1.4 \times 10^{-11}$ J/m, while for the simulation on stripe period, we chose the exchange stiffness A_{ex} in the range between 7×10^{-12} J/m and 1.12×10^{-10} J/m to see how the period of stripes changes with A_{ex}. We chose the damping coefficient α for faster responser in our simulation. There is no Dzyaloshiskii−Moriya interaction, so the stripes and skymions resulted from only the interplay between dipolar field, exchange, and anisotropy. The initial configurations were prepared by annealing from high transverse field to low transverse field (2 mT), so the direction of the stripes and the in-plane magnetization is pinned along the field direction. For the simulation on skyrmion formation, the systems have varying thicknesses along the x direction, shown in Figure S7. In contrast, the thickness in stripe width simulations is uniform, shown in Figure 2 and Figure S1. Periodic boundary conditions were used along the y-axis, while the x-axis and z-axis had open boundary conditions. It should be noted that our simulations are limited by time and computational power. Thus, it is impossible to simulate on the same time scale as experiments. In addition, the model is course-grained, discretized, and finite-sized, so the simulation time scale could not be related to the real experiment directly. However, qualitative study of the trend gives us insight into the mechanism.

ASSOCIATED CONTENT

Supporting Information

The Supporting Information is available free of charge at https://pubs.acs.org/doi/10.1021/acsnano.1c04053.

Relations between exchange stiffness, pitch length, and thickness at phase transition in micromagnetic simulation and experiments; effect of the magnetic field strength on magnetic texture transformation during in-plane field oscillation; LTEM images of the in-plane field induced magnetic transformation; additional micromagnetic simulation results of skyrmion formation and their stability to varied thickness gradients in Fe_3Sn_2 (PDF)

Movie S1 showing the dynamic transformation between magnetic bubbles and stripes during an in-plan field oscillation process (MP4)

Movie S2 showing the micromagnetic simulation of the stability of magnetic bubbles nucleated at the magnetic stripe domain boundary with thickness gradient (128 to 90 nm) with a field variation of 2 mT to −10 mT in 400 ns (MP4)

Movie S3 showing micromagnetic simulation of the stability of magnetic bubbles nucleated at the magnetic stripe domain boundary with thickness gradient (160 to 75 nm) with a field variation of 2 mT to −10 mT in 400 ns (MP4)

Movie S4 showing micromagnetic simulation of the stability of magnetic bubbles nucleated at the magnetic

https://doi.org/10.1021/acsnano.1c04053
ACS Nano 2021, 15, 13495−13503

stripe domain boundary with thickness gradient (128 to 90 nm) with a field variation of 2 mT to −10 mT in 800 ns (MP4)

Movie S5 showing LTEM movie of the transformation of magnetic textures during an in-plan field oscillation process (MP4)

Movie S6 showing LTEM Movie of the transformation of a magnetic skyrmion-like texture to stripe like texture during an in-plan field oscillation process (MP4)

AUTHOR INFORMATION

Corresponding Author

David W. McComb − *Department of Materials Science and Engineering and Center for Electron Microscopy and Analysis, The Ohio State University, Columbus, Ohio 43212, United States*; Email: mccomb.29@osu.edu

Authors

Binbin Wang − *Department of Materials Science and Engineering and Center for Electron Microscopy and Analysis, The Ohio State University, Columbus, Ohio 43212, United States*; orcid.org/0000-0003-0419-6234

Po-kuan Wu − *Department of Physics, The Ohio State University, Columbus, Ohio 43210, United States*

Núria Bagués Salguero − *Department of Materials Science and Engineering and Center for Electron Microscopy and Analysis, The Ohio State University, Columbus, Ohio 43212, United States*

Qiang Zheng − *Materials Science and Technology Division, Oak Ridge National Laboratory, Oak Ridge, Tennessee 37831, United States; Department of Materials Science and Engineering, University of Tennessee, Knoxville, Tennessee 37996, United States*

Jiaqiang Yan − *Materials Science and Technology Division, Oak Ridge National Laboratory, Oak Ridge, Tennessee 37831, United States; Department of Materials Science and Engineering, University of Tennessee, Knoxville, Tennessee 37996, United States*

Mohit Randeria − *Department of Physics, The Ohio State University, Columbus, Ohio 43210, United States*

Complete contact information is available at: https://pubs.acs.org/10.1021/acsnano.1c04053

Author Contributions

B.W. and D.W.M. conceived the project; B.W. designed and performed experiments; N.B. assisted with the material characterization; P.W. and M.R. conducted the micromagnetic modeling and analysis; Q.Z. and J.Y. grew the single crystal of Fe_3Sn_2. B.W. drafted the manuscript with the help of N.B. and P.Wu., then the manuscript was revised by D.W.M and M.R. All authors have given approval to the final version of the manuscript.

Notes

The authors declare no competing financial interest.

ACKNOWLEDGMENTS

We thank A. Wade and R. Williams for their assistance with the TEM and helpful discussions. This work was primarily supported by DARPA under Grant No. D18AP00008. Partial support by the Center for Emergent Materials at The Ohio State University, an NSF MRSEC (DMR-2011876) is acknowledged. Electron microscopy experiments were supported by the Center for Electron Microscopy and Analysis at the Ohio State University. Work at ORNL was supported by the U.S. Department of Energy, Office of Science, Basic Energy Sciences, Materials Sciences and Engineering Division.

REFERENCES

(1) Nagaosa, N.; Tokura, Y. Topological Properties and Dynamics of Magnetic Skyrmions. *Nat. Nanotechnol.* **2013**, *8* (12), 899−911.

(2) Zhang, X.; Zhou, Y.; Song, K. M.; Park, T. E.; Xia, J.; Ezawa, M.; Liu, X.; Zhao, W.; Zhao, G.; Woo, S. Skyrmion-Electronics: Writing, Deleting, Reading and Processing Magnetic Skyrmions toward Spintronic Applications. *J. Phys.: Condens. Matter* **2020**, *32*, 143001.

(3) Heinze, S.; Von Bergmann, K.; Menzel, M.; Brede, J.; Kubetzka, A.; Wiesendanger, R.; Bihlmayer, G.; Blügel, S. Spontaneous Atomic-Scale Magnetic Skyrmion Lattice in Two Dimensions. *Nat. Phys.* **2011**, *7* (9), 713−718.

(4) Okubo, T.; Chung, S.; Kawamura, H. Multiple-q States and the Skyrmion Lattice of the Triangular-Lattice Heisenberg Antiferromagnet under Magnetic Fields. *Phys. Rev. Lett.* **2012**, *108* (1), 017206.

(5) Leonov, A. O.; Mostovoy, M. Multiply Periodic States and Isolated Skyrmions in an Anisotropic Frustrated Magnet. *Nat. Commun.* **2015**, *6* (1), 1−8.

(6) Yu, X.; Mostovoy, M.; Tokunaga, Y.; Zhang, W.; Kimoto, K.; Matsui, Y.; Kaneko, Y.; Nagaosa, N.; Tokura, Y. Magnetic Stripes and Skyrmions with Helicity Reversals. *Proc. Natl. Acad. Sci. U. S. A.* **2012**, *109* (23), 8856−8860.

(7) Hirschberger, M.; Nakajima, T.; Gao, S.; Peng, L.; Kikkawa, A.; Kurumaji, T.; Kriener, M.; Yamasaki, Y.; Sagayama, H.; Nakao, H.; Ohishi, K.; Kakurai, K.; Taguchi, Y.; Yu, X.; Arima, T.-h.; Tokura, Y. Skyrmion Phase and Competing Magnetic Orders on a Breathing Kagomé Lattice. *Nat. Commun.* **2019**, *10* (1), 1−9.

(8) Hou, Z.; Zhang, Q.; Xu, G.; Gong, C.; Ding, B.; Wang, Y.; Li, H.; Liu, E.; Xu, F.; Zhang, H.; Yao, Y.; Wu, G.; Zhang, X. X.; Wang, W. Creation of Single Chain of Nanoscale Skyrmion Bubbles with Record-High Temperature Stability in a Geometrically Confined Nanostripe. *Nano Lett.* **2018**, *18* (2), 1274−1279.

(9) Hou, Z.; Ren, W.; Ding, B.; Xu, G.; Wang, Y.; Yang, B.; Zhang, Q.; Zhang, Y.; Liu, E.; Xu, F.; Wang, W.; Wu, G.; Zhang, X.; Shen, B.; Zhang, Z. Observation of Various and Spontaneous Magnetic Skyrmionic Bubbles at Room Temperature in a Frustrated Kagome Magnet with Uniaxial Magnetic Anisotropy. *Adv. Mater.* **2017**, *29* (29), 1701144.

(10) Tang, J.; Kong, L.; Wu, Y.; Wang, W.; Chen, Y.; Wang, Y.; Li, J.; Soh, Y.; Xiong, Y.; Tian, M.; Du, H. Target Bubbles in Fe_3Sn_2 Nanodisks at Zero Magnetic Field. *ACS Nano* **2020**, *14* (9), 10986−10992.

(11) Yu, X.; Tokunaga, Y.; Taguchi, Y.; Tokura, Y. Variation of Topology in Magnetic Bubbles in a Colossal Magnetoresistive Manganite. *Adv. Mater.* **2017**, *29* (3), 1603958.

(12) Wang, W.; Zhang, Y.; Xu, G.; Peng, L.; Ding, B.; Wang, Y.; Hou, Z.; Zhang, X.; Li, X.; Liu, E.; Wang, S.; Cai, J.; Wang, F.; Li, J.; Hu, F.; Wu, G.; Shen, B.; Zhang, X.-X. A Centrosymmetric Hexagonal Magnet with Superstable Biskyrmion Magnetic Nanodomains in a Wide Temperature Range of 100−340 K. *Adv. Mater.* **2016**, *28* (32), 6887−6893.

(13) Sun, L.; Cao, R. X.; Miao, B. F.; Feng, Z.; You, B.; Wu, D.; Zhang, W.; Hu, A.; Ding, H. F. Creating an Artificial Two-Dimensional Skyrmion Crystal by Nanopatterning. *Phys. Rev. Lett.* **2013**, *110* (16), 167201.

(14) Hou, Z.; Zhang, Q.; Xu, G.; Zhang, S.; Gong, C.; Ding, B.; Li, H.; Xu, F.; Yao, Y.; Liu, E.; Wu, G.; Zhang, X. X.; Wang, W. Manipulating the Topology of Nanoscale Skyrmion Bubbles by Spatially Geometric Confinement. *ACS Nano* **2019**, *13* (1), 922−929.

(15) Jiang, W.; Upadhyaya, P.; Zhang, W.; Yu, G.; Jungfleisch, M. B.; Fradin, F. Y.; Pearson, J. E.; Tserkovnyak, Y.; Wang, K. L.; Heinonen, O.; Te Velthuis, S. G. E.; Hoffmann, A. Blowing Magnetic Skyrmion Bubbles. *Science* **2015**, *349* (6245), 283−286.

(16) Yu, X.; Morikawa, D.; Tokunaga, Y.; Kubota, M.; Kurumaji, T.; Oike, H.; Nakamura, M.; Kagawa, F.; Taguchi, Y.; Arima, T. H.; Kawasaki, M.; Tokura, Y. Current-Induced Nucleation and Annihilation of Magnetic Skyrmions at Room Temperature in a Chiral Magnet. *Adv. Mater.* **2017**, *29* (21), 1606178.
(17) Finazzi, M.; Savoini, M.; Khorsand, A. R.; Tsukamoto, A.; Itoh, A.; Duò, L.; Kirilyuk, A.; Rasing, T.; Ezawa, M. Laser-Induced Magnetic Nanostructures with Tunable Topological Properties. *Phys. Rev. Lett.* **2013**, *110* (17), 177205.
(18) Yin, J. X.; Zhang, S. S.; Li, H.; Jiang, K.; Chang, G.; Zhang, B.; Lian, B.; Xiang, C.; Belopolski, I.; Zheng, H.; Cochran, T. A.; Xu, S. Y.; Bian, G.; Liu, K.; Chang, T. R.; Lin, H.; Lu, Z. Y.; Wang, Z.; Jia, S.; Wang, W.; et al. Giant and Anisotropic Many-Body Spin−Orbit Tunability in a Strongly Correlated Kagome Magnet. *Nature* **2018**, *562* (7725), 91−95.
(19) Ye, L.; Kang, M.; Liu, J.; Von Cube, F.; Wicker, C. R.; Suzuki, T.; Jozwiak, C.; Bostwick, A.; Rotenberg, E.; Bell, D. C.; Fu, L.; Comin, R.; Checkelsky, J. G. Massive Dirac Fermions in a Ferromagnetic Kagome Metal. *Nature* **2018**, *555* (7698), 638−642.
(20) Kang, M.; Ye, L.; Fang, S.; You, J. S.; Levitan, A.; Han, M.; Facio, J. I.; Jozwiak, C.; Bostwick, A.; Rotenberg, E.; Chan, M. K.; McDonald, R. D.; Graf, D.; Kaznatcheev, K.; Vescovo, E.; Bell, D. C.; Kaxiras, E.; van den Brink, J.; Richter, M.; Prasad Ghimire, M.; et al. Dirac Fermions and Flat Bands in the Ideal Kagome Metal FeSn. *Nat. Mater.* **2020**, *19* (2), 163−169.
(21) Han, M. G.; Garlow, J. A.; Liu, Y.; Zhang, H.; Li, J.; Dimarzio, D.; Knight, M. W.; Petrovic, C.; Jariwala, D.; Zhu, Y. Topological Magnetic-Spin Textures in Two-Dimensional van der Waals $Cr_2Ge_2Te_6$. *Nano Lett.* **2019**, *19* (11), 7859−7865.
(22) Prosen, R. J.; Holmen, J. O.; Gran, B. E. Rotatable Anisotropy in Thin Permalloy Films. *J. Appl. Phys.* **1961**, *32*, 91.
(23) Lommel, J. M.; Graham, C. D. Rotatable Anisotropy in Composite Films. *J. Appl. Phys.* **1962**, *33* (3), 1160−1161.
(24) Garnier, L.-C.; Marangolo, M.; Eddrief, M.; Bisero, D.; Fin, S.; Casoli, F.; Pini, M. G.; Rettori, A.; Tacchi, S. Stripe Domains Reorientation in Ferromagnetic Films with Perpendicular Magnetic Anisotropy. *J. Phys. Mater.* **2020**, *3* (2), 024001.
(25) Tacchi, S.; Fin, S.; Carlotti, G.; Gubbiotti, G.; Madami, M.; Barturen, M.; Marangolo, M.; Eddrief, M.; Bisero, D.; Rettori, A.; Pini, M. G. Rotatable Magnetic Anisotropy in a $Fe_{0.8}$ $Ga_{0.2}$ Thin Film with Stripe Domains: Dynamics ee Statics. *Phys. Rev. B: Condens. Matter Mater. Phys.* **2014**, *89* (2), 024411.
(26) Romming, N.; Hanneken, C.; Menzel, M.; Bickel, J. E.; Wolter, B.; Von Bergmann, K.; Kubetzka, A.; Wiesendanger, R. Writing and Deleting Single Magnetic Skyrmions. *Science* **2013**, *341* (6146), 636−639.
(27) Yoshimura, Y.; Kim, K. J.; Taniguchi, T.; Tono, T.; Ueda, K.; Hiramatsu, R.; Moriyama, T.; Yamada, K.; Nakatani, Y.; Ono, T. Soliton-like Magnetic Domain Wall Motion Induced by the Interfacial Dzyaloshinskii-Moriya Interaction. *Nat. Phys.* **2016**, *12* (2), 157−161.
(28) Peng, L.; Takagi, R.; Koshibae, W.; Shibata, K.; Nakajima, K.; Arima, T.-h.; Nagaosa, N.; Seki, S.; Yu, X.; Tokura, Y. Controlled Transformation of Skyrmions and Antiskyrmions in a Non-Centrosymmetric Magnet. *Nat. Nanotechnol.* **2020**, *15* (3), 181−186.
(29) Yan, J. Q.; Sales, B. C.; Susner, M. A.; McGuire, M. A. Flux Growth in a Horizontal Configuration: An Analog to Vapor Transport Growth. *Phys. Rev. Mater.* **2017**, *1* (2), 023402.
(30) Egerton, R. F. *Electron Energy-Loss Spectroscopy in the Electron Microscope*, 3rd ed.; Springer: New York, 2011.
(31) Ishizuka, K.; Allman, B. Phase Measurement of Atomic Resolution Image Using Transport of Intensity Equation. *Microscopy (Oxford, U. K.)* **2005**, *54* (3), 191−197.

https://doi.org/10.1021/acsnano.1c04053
ACS Nano 2021, 15, 13495−13503